DOI: 10.13009/EUCASS2019-960

DOI: ADD DOINUMBER HERE

Guidance Algorithm for Low-lift Skip Entry Based on Linear Pseudospectral Model Predictive Control

Wenhao Du[⋆†]*, Wanchun Chen*[⋆]*, Hao Zhou*[⋆]*, and Liang Yang*[⋆]
[⋆]*School of Astronautics, Beihang University*
No. 37 Xueyuan Road, Haidian District, Beijing, China
duwenhao@buaa.edu.cn · wanchun_chen@buaa.edu.cn
zhouhao.buaa@hotmail.com · yangliang2016@buaa.edu.cn
[†]Corresponding author

Abstract

A closed-loop guidance algorithm is proposed for low lift-to-drag vehicles in the skip entry flight. Firstly, perturbation equations are obtained for the normal entry dynamical system with a rotating Earth. Then, Gauss collocation method is applied to transfer these dynamic constraints to linear algebraic equations. Thus, the modification of control parameters is analytically expressed in terms of terminal state errors by deriving the transfer matrix. Compared with the previous studies, the method proposed in this paper is able to preset the number of bank reversals and the exact reversal time, thereby reducing the control complexity significantly.

1. Introduction

The entry guidance plays an important role in the lunar return missions, and for entry vehicles with relatively low-lift-to-drag (L/D) ratios such as Orion Crew Exploration Vehicle, skip entry strategy allows a long downrange so that more landing sites can be covered to avoid bad weather conditions. Fig. (1) illustrates this concept with the skip phase, the Kepler phase, and the final phase. Since the Apollo era,[2] people have realized that the skip trajectory would need to be designed based on the current flight state. Because of the limited on-board computation at the time, the magnitude of bank angle in the skip phase is determined by analytical expressions based on approximations and empirical equations. The adjoint method is applied in the final phase to estimate the downrange by generating the trajectory sensitivity coefficients. However, the various simplifications significantly limit guidance accuracy, especially for the case with a long downrange. Although a skip entry flight has never been flown in the Apollo program, the final phase guidance algorithm is used in the subsequent studies of Orion spacecraft. A predictor-corrector algorithm, PreGuid[8–11]is designed to replace the Apollo's reference-following skip guidance with the purpose of extending the range. Hence, PreGuid is able to satisfy the maximum range, 1000 km, of in the Orion design concept, whereas the maximum entry range of a manned Apollo capsule in an actual flight is 3400 km.[7] Although the adoption of PreGuid for Orion demonstrates the feasibility of a new-generation of algotrithms, it should be mentioned that the final phase guidance of PreGuid is nearly the same as that used in Apollo program. Brunner and Lu further provided a fully numerical predictor-corrector guidance algorithm that is applicable for both skip and final phase.[1,4,5] In the longitudinal plane, the downrange requirement is satisfied by determining a linear bank angle magnitude, and the lateral guidance follows the Apollo bank reversal logic which keeps the crossrange in an envelope and steers the vehicle to the landing site. In recent years, numerical predict-corrector guidance algorithms[12,14] have been widely designed and implemented for skip entry problem. Although the combination of numerical prediction and feed-back error correction have demonstrated the efficiency and robustness of this method in the longitudinal guidance, the lateral control logic is still based on the Apollo lateral logic. However, the number of bank reversals and the specific bank reversal time can not be predetermined and predicted, which increases the uncertainty to actual flight. Furthermore, the state errors can be amplified by the long Kepler phase. Hence, it is difficult for the guidance law based on traditional lateral logic to precisely estimate the second entry point and provide a good initial conditions for the final phase. Although Brunner and Lu[1] applied targeting bias to compensate for the Earth rotation, but the lateral error of the second entry point is unknown and this method performance relies on empirical results.[6] Although Kelly[3] presented a closed-loop bank reversal method that operates with a fixed number of bank reversals, the bank reversal time is still non-deterministic.

DOI: 10.13009/EUCASS2019-960

A closed-loop guidance algorithm that eliminates the terminal downrange and crossrange errors by modifying the magnitude of bank angle and regulating the reversal time respectively is proposed for low lift-to-drag vehicles in the skip entry phase of a lunar-return mission. Firstly, perturbation equations are obtained by applying the linearization method to the normal entry dynamical system with a spherical and rotating Earth as well as coupled lateral and longitudinal motions. Then, these dynamical constraints are discretized into a group of linear algebraic equations using Gauss Pseudospectral method. Therefore, boundary variations can be expressed by the state variations at the Gauss collocation points and the initial point combining with the trajectory integration and Gauss quadrature.[13] After formulating the initial state deviation as a function of the reversal time according to Calculus of variations, we successfully derive an analytical formula to update control parameters including the bank angle magnitude and bank reversal commands. Compared with the traditional guidance logic where a heading error deadband is defined to provide the maximum allowable error, the method proposed in this paper is able to prescribe the reversal time, so that only a few numbers of bank reversals are needed in the skip phase, thereby reducing the control complexity. The performance of the proposed method is assessed by dispersion simulations and comparison with other methods. The results show that this method is not only accuracy mathematically, but also has strong robustness, and excellent performance.

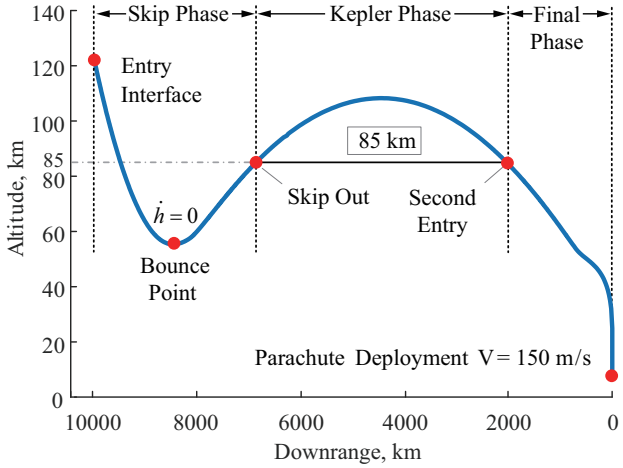

Figure 1: Segments of the skip entry trajectory.

2. Problem formulation

2.1 Dynamic model

The dimensionless equations of three-degree-of-freedom motion of a gliding vehicle inside the atmosphere of a spherical, rotating Earth can be described as

$$\dot{r} = V\sin\gamma, \tag{1}$$

$$\dot{\theta} = \frac{V\cos\gamma\sin\psi}{r\cos\phi}, \tag{2}$$

$$\dot{\phi} = \frac{V\cos\gamma\cos\psi}{r}, \tag{3}$$

$$\dot{V} = -D - \frac{\sin\gamma}{r^2} + C_V, \tag{4}$$

$$\dot{\gamma} = \frac{1}{V}\left[L\cos\sigma + \left(V^2 - \frac{1}{r}\right)\frac{\cos\gamma}{r} + C_\gamma\right], \tag{5}$$

$$\dot{\psi} = \frac{1}{V}\left[\frac{L\sin\sigma}{\cos\gamma} + \frac{V^2}{r}\cos\gamma\sin\psi\tan\phi + C_\psi\right], \tag{6}$$

DOI: 10.13009/EUCASS2019-960

with

$$\begin{aligned} C_V &= \Omega^2 r\cos\phi\left(\sin\gamma\cos\phi-\cos\gamma\sin\phi\cos\psi\right), \\ C_\gamma &= 2\Omega V\cos\phi\sin\psi+\Omega^2 r\cos\phi\left(\cos\gamma\cos\phi+\sin\gamma\cos\psi\sin\phi\right), \\ C_\psi &= -2\Omega V\left(\tan\gamma\cos\psi\cos\phi-\sin\phi\right)+\Omega^2 r\sin\psi\sin\phi\cos\phi/\cos\gamma, \end{aligned} \tag{7}$$

where the differentiations in Eqs.(1)-(6) are with respect to a dimensionless time $\tau = t/t_{scale}$, t is the flight time and $t_{scale} = \sqrt{R_0/g_0}$ is a scaling factor, R_0 is the radius of Earth, g_0 is the gravitational acceleration at the Earth's surface. r is the radial distance from the Earth's center to the vehicle and then scaled by R_0, θ and ϕ are the longitude and geocentric latitude, respectively. V is the planet-relative velocity and nondimensionalized by the $V_{scale} = \sqrt{R_0 g_0}$, γ is the flight-path angle, and ψ is the heading angle measured clockwise in the local horizontal plane form the north. The roll angle of the relative velocity vector is denoted as the bank angle σ, which is measured positive for starboard tacks. C_V, C_γ, and C_ψ account for the contribution of Coriolis acceleration and convected acceleration, the self-rotation rate of the Earth is $\Omega = 7.2921151e^{-5} rad/s$ and then scaled by t_{scale}. The terms L and D are the aerodynamic lift and drag acceleration which can be expressed as

$$L = \frac{\rho V^2 C_L S_{ref}}{2mg_0}, \quad D = \frac{\rho V^2 C_D S_{ref}}{2mg_0}, \tag{8}$$

where ρ is the local atmospheric density, C_L and C_D are the lift and drag coefficients which are only dependent on the AOA and Mach number. S_{ref} and m denote the vehicle's mass and reference area, respectively.

2.2 Boundary constraints

The initial conditions of a skip entry usually correspond to those of a lunar-return mission, and are given as

$$X_0 = [r_0, \theta_0, \phi_0, V_0, \gamma_0, \psi_0]. \tag{9}$$

For the terminal conditions, a specified relative velocity is adopted to terminate the simulation, since the parachute will be deployed before the low-L/D vehicle touches down. In this paper, $V_f = 150\ m/s$, which is the same with that in[1] for the convenience of comparison.

2.3 Vehicle model

The vehicle model considered in this paper is similar to that of the Orion Crew Exploration Vehicle, which has an axisymmetric blunt body close to the Apollo capsule. In order to keep the vehicle in a trim condition, the trim angle of attack (α_{trim}) is designed to change with Mach number.In the skip phase, α_{trim} is around 160°, which results in a L/D about 0.288. The orientation of aerodynamic lift is rotated using a bank angle modulation strategy, in which the maximum rate and acceleration in the 3-DOF simulations are set to $20 deg/s$ and $10 deg/s^2$, respectively.

3. Guidance law

3.1 Control Parameterization

In the designing of the guidance algorithm for skip entry, the magnitude and reversal time of the bank angle need to be collocated circumspectly in order to satisfy the longitudinal and lateral constraints simultaneously. The magnitude is parameterized as a piecewise linear function of the flight time as shown in Fig. 2. t_{k1} and t_{k2} denote the initial and final points of Kepler phase respectively, which both correspond to the height of $85km$. The threshold value t_h is set to be a constant between t_{k1} and t_{k2}, so that more flexibility can be provided in the skip phase and the Reaction Control System (RCS) propellant consumption can be reduced in the Kepler phase. Therefore, the bank angle magnitude at any flight time $t \le t_h$ can be expressed as a linear function

$$f(t) = \sigma_f + \frac{\sigma_0 - \sigma_f}{t_h}\left(t_h - t\right), \quad t \le t_h$$

where $\sigma_f = 70 deg$ is a fixed constant magnitude applied for $t \ge t_h$.

In addition to the modulation of $|\sigma|$, two bank reversals are arranged in the skip phase. One is performed next to the bounce point so as to make full use of the aerodynamic force to eliminate lateral errors effectively, and the other

DOI: 10.13009/EUCASS2019-960

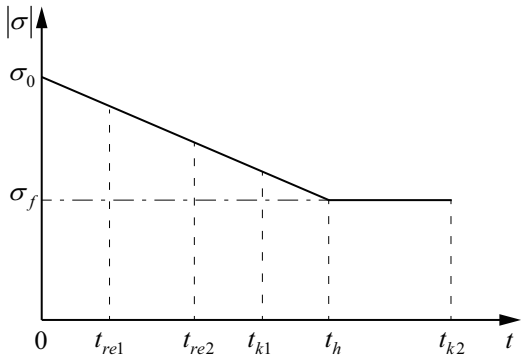

Figure 2: Piecewise bank-vs-time profile in skip phase.

one is done near the skip out point with the purpose of reducing the accumulated longitudinal and lateral errors during the Kepler phase. Ultimately, the expression of bank angle is defined in four intervals as follows

$$\sigma = \begin{cases} \mp f(t), & t_0 \le t \le t_{re1} \\ \pm f(t), & t_{re1} \le t \le t_{re2} \\ \mp f(t), & t_{re2} \le t \le t_h \\ \mp \sigma_f, & t_h \le t \le t_f \end{cases} \tag{10}$$

where the sign of bank angle in the second phase is opposite to those in other segments because of the bank reversal maneuver. Consequently, the bank angle is parameterized as a piecewise function of the initial magnitude, σ_0, and the bank reversal time, t_{re1} and t_{re2}. Then, we will formulate the analytical relation between the modification of these control parameters and the adjustment of terminal states, so that a series of analytical correction formulas can be designed to eliminate the final errors.

3.2 Analysis of the initial magnitude

In this subsection, the relation with the modification of initial magnitude $\delta\sigma_0$ is derived by incorporating the Gauss collocation method with the model predictive control. It should be noted that the variation of t_{re1} and t_{re2} will be discussed later, thus the bank reversal time is considered as constants in the derivation process. Firstly, a series of linear dynamics with regard to the variation of state is formulated. Then, combining with the Gauss collocation method, the terminal dispersions can be explicitly expressed as the function of σ_0. Hence, a feedback control law at the current time can be determined to update the initial magnitude.

Let us consider the entry dynamics with final constraints, which can be generally formulated as follows

$$\begin{aligned} \dot{\mathbf{x}} &= \mathbf{f}^{(1)}(\mathbf{x}, u, t) \\ \varphi\left(\mathbf{x}\left(t_f\right)\right) &= \mathbf{0} \end{aligned} \tag{11}$$

where $\mathbf{x} = [r, \theta, \phi, V, \gamma, \psi]^T$ is the state vector, $u = \sigma$ is the control variable, and φ denotes the terminal constraints. If the initial guess u_{ref} is given, the whole skip trajectory and the reference state $\mathbf{x}_{ref}$ can be simulated onboard using numerical integration methods, such as the fourth-order Runge-Kutta scheme. Then, perturbation equations can be formulated by linearizing Eq. (11) around the reference trajectory:

$$\delta\dot{\mathbf{x}} = \widehat{\mathbf{A}}\delta\mathbf{x} + \widehat{\mathbf{B}}\delta u \tag{12}$$

where $\delta\mathbf{x} = \mathbf{x} - \mathbf{x}_{ref}$, $\delta u = u - u_{ref}$, f_x and f_u are the partial derivatives of entry dynamics f with respect to state and control respectively. Furthermore, f_x is a coefficient matrix of 6×6, f_u is a column vector of 6×1,

$$\widehat{\mathbf{A}} = \begin{bmatrix} 0 & 0 & 0 & a_{14} & a_{15} & 0 \\ a_{21} & 0 & a_{23} & a_{24} & a_{25} & a_{26} \\ a_{31} & 0 & 0 & a_{34} & a_{35} & a_{36} \\ a_{41} & 0 & a_{43} & a_{44} & a_{45} & a_{46} \\ a_{51} & 0 & a_{53} & a_{54} & a_{55} & a_{56} \\ a_{61} & 0 & a_{63} & a_{64} & a_{65} & a_{66} \end{bmatrix}, \quad \widehat{\mathbf{B}} = \begin{bmatrix} 0 \\ 0 \\ 0 \\ 0 \\ b_{51} \\ b_{61} \end{bmatrix}. \tag{13}$$

DOI: 10.13009/EUCASS2019-960

Analytical expressions of all the parameters are given in 4. Moreover, since the control variable has been parametrized as the continuous function of the flight time in Eq. (10), the variation of control reduces to

$$\delta u = \delta\sigma = \begin{cases} \mp\left(1 - t/t_h\right)\delta\sigma_0 & t_0 \le t \le t_{re1}, \\ \pm\left(1 - t/t_h\right)\delta\sigma_0 & t_{re1} \le t \le t_{re2}, \\ \mp\left(1 - t/t_h\right)\delta\sigma_0 & t_{re2} \le t \le t_h, \\ 0 & t_h \le t \le t_f. \end{cases} \tag{14}$$

It is apparent form Eqs. (12) and (14) that the the variable of terminal state $\delta\mathbf{x}_f$ can be determined by solving the linear dynamics in Eq. (12), once the correction of control parameter $\delta\sigma_0$ is given. Recall that orthogonal collocation methods can transcribe continuous-time differential equations to finite-dimensional algebraic equations, but the Legendre-Gauss (LG) points used in the Gauss pseudospectral method are defined on the interval $[-1, +1]$, hence the four subintervals of the time domain $[t_0, t_f]$ are firstly mapped to $[-1, +1]$ by using the following affine transformation

$$t = \frac{t_k - t_{k-1}}{2}\tau + \frac{t_k + t_{k-1}}{2}, \quad k = 1, 2, 3, 4, \tag{15}$$

with

$$\begin{bmatrix} t_1 & t_2 & t_3 & t_4 \end{bmatrix} = \begin{bmatrix} t_{re1} & t_{re2} & t_h & t_f \end{bmatrix}.$$

where the subscript k denotes the *kth* interval.

Use the mapping to convert the linear dynamics given in Eq. (12) to the time domain $\tau \in [-1, +1]$, and replace δu by Eq. (14), we have

$$\frac{d}{d\tau}\delta\mathbf{x}^{(k)} = \mathbf{A}^{(k)}(\tau)\delta\mathbf{x}^{(k)} + \mathbf{B}^{(k)}(t)\delta\sigma_0, \quad k = 1, 2, 3, 4, \tag{16}$$

with

$$\begin{aligned} \mathbf{A}^{(k)} &= \frac{t_k - t_{k-1}}{2}\widehat{\mathbf{A}}^{(k)} \qquad k = 1, 2, 3, 4, \\ \mathbf{B}^{(k)} &= \begin{cases} \mp\dfrac{t_k - t_{k-1}}{2}\left(1 - \dfrac{t}{t_h}\right)\widehat{\mathbf{B}}^{(k)} & k = 1, 2, 3, \\ \mathbf{0} & k = 4. \end{cases} \end{aligned} \tag{17}$$

where the boldface symbol $\mathbf{0}$ is a column vector of zeros. It should be noted that the sign of $\mathbf{B}^{(2)}$ is opposite to those of $\mathbf{B}^{(1)}$ and $\mathbf{B}^{(3)}$, because of bank reversals.

Then, a Lagrange polynomial using the initial point, $\tau_0^{(k)} = -1$, and the LG points, $\left(\tau_1^{(k)}, \cdots, \tau_{N_k}^{(k)}\right)$, where the subscript N_k denotes the number of collocation points in interval k, is applied to approximate the variation of state

$$\delta\mathbf{x}^{(k)}(\tau) \approx \delta\mathbf{X}^{(k)}(\tau) = \sum_{j=0}^{N_k} \delta\mathbf{X}_j^{(k)} L_j^{(k)}(\tau), \quad \delta\mathbf{X}_j^{(k)} = \delta\mathbf{X}^{(k)}(\tau_j^{(k)}), \tag{18}$$

where $L^{(k)}$ denotes the Lagrange basis associated with the $\tau_i^{(k)}$

$$L_j^{(k)}(\tau) = \prod_{\substack{i=0 \\ i \ne j}}^{N_k} \frac{\tau - \tau_i^{(k)}}{\tau_j^{(k)} - \tau_i^{(k)}}, \quad 0 \le j \le N.$$

Differentiating Eq. (18) and evaluating the result at the collocation point gives

$$\frac{d}{d\tau}\delta\mathbf{X}^{(k)}(\tau_i^{(k)}) = \sum_{j=0}^{N_k} \delta\mathbf{X}_j^{(k)} \dot{L}_j^{(k)}(\tau_i^{(k)}) = \sum_{j=0}^{N_k} \widehat{D}_{ij}^{(k)} \delta\mathbf{X}_j^{(k)}, 1 \le i \le N_k$$

The differential matrix $\widehat{\mathbf{D}}^{(k)} = [\widehat{\mathbf{D}}_0^{(k)} \quad \widehat{\mathbf{D}}_{1:N_k}^{(k)}]$ is a $N_k \times (N_k + 1)$ non-square matrix, where $\widehat{\mathbf{D}}_0^{(k)}$ is the first column of $\widehat{\mathbf{D}}^{(k)}$ and $\widehat{\mathbf{D}}_{1:N_k}^{(k)}$ denotes the remaining N_k columns. As shown in ref1, $\widehat{\mathbf{D}}_{1:N_k}^{(k)}$ is invertible.

Next, we can form the discrete dynamics for interval k by collocating the derivative of $\delta\mathbf{X}^{(k)}(\tau)$ with the right hand side of the linear dynamics of Eq. (16) at the N_k LG points as

$$\delta\dot{\mathbf{X}}_{1:N_k}^{(k)} = \mathbf{D}_0^{(k)}\delta\mathbf{X}_0^{(k)} + \mathbf{D}_{1:N_k}^{(k)}\delta\mathbf{X}_{1:N_k}^{(k)} = \mathbf{A}_{1:N_k}^{(k)}\delta\mathbf{X}_{1:N_k}^{(k)} + \mathbf{B}_{1:N_k}^{(k)}\delta\sigma_0 \tag{19}$$

DOI: 10.13009/EUCASS2019-960

with

$$\left[\mathbf{D}_0^{(k)} \quad \mathbf{D}_{1:N_k}^{(k)}\right] = \left[\widehat{\mathbf{D}}_0^{(k)} \quad \widehat{\mathbf{D}}_{1:N_k}^{(k)}\right] \otimes \mathbf{I}_n$$

where $\otimes$ denotes the Kronecker product, $\mathbf{I}_n$ is an identity matrix of size $n \times n$ and n is the number of states, $\mathbf{A}_{1:N_k}^{(k)}$ is a $nN_k \times nN_k$ diagonal matrix with diagonal elements $\mathbf{A}^{(k)}(\tau_i^{(k)})$, $i = 1, \cdots, N_k$, while $\delta\mathbf{X}_{1:N_k}^{(k)}$, $\delta\dot{\mathbf{X}}_{1:N_k}^{(k)}$, and $\mathbf{B}_{1:N_k}^{(k)}$ are $nN_k \times 1$ column vectors consisted of $\delta\mathbf{X}_i^{(k)}$, $\delta\dot{\mathbf{X}}^{(k)}(\tau_i^{(k)})$, and $\mathbf{B}^{(k)}(\tau_i^{(k)})$, $i = 1, \cdots, N_k$, respectively.

On the other hand, let $\delta\mathbf{X}_{N_k+1}^{(k)}$ be the approximation of the variable of state at $\tau_{N_k+1}^{(k)} = +1$. It follows from the LG quadrature rule that

$$\begin{aligned}\delta\mathbf{X}_{N_k+1}^{(k)} &= \delta\mathbf{X}_0^{(k)} + \sum_{i=1}^{N_k} w_i^{(k)} \delta\dot{\mathbf{X}}^{(k)}(\tau_i^{(k)}) \\ &= \delta\mathbf{X}_0^{(k)} + \mathbf{W}^{(k)}\left(\mathbf{A}_{1:N_k}^{(k)}\delta\mathbf{X}_{1:N_k}^{(k)} + \mathbf{B}_{1:N_k}^{(k)}\delta\sigma_0\right),\end{aligned} \tag{20}$$

where $w_i^{(k)}$, $1 \le i \le N_k$ are the Gauss quadrature weights in interval k, and $\mathbf{W}^{(k)}$ denotes a $n \times nN_k$ coefficient matrix

$$\mathbf{W}^{(k)} = \left[w_1^{(k)} \quad w_2^{(k)} \quad \cdots \quad w_{N_k}^{(k)}\right] \otimes \mathbf{I}_n$$

Rearranging Eq. (19) gives

$$\delta\mathbf{X}_{1:N_k}^{(k)} = \left(\mathbf{D}_{1:N_k}^{(k)} - \mathbf{A}_{1:N_k}^{(k)}\right)^{-1}\left(\mathbf{B}_{1:N_k}^{(k)}\delta\sigma_0 - \mathbf{D}_0^{(k)}\delta\mathbf{X}_0^{(k)}\right) \tag{21}$$

Replace the $\delta\mathbf{X}_{1:N_k}^{(k)}$ in Eq. (20) by Eq. (21) to obtain the explicit expression of $\delta\mathbf{X}_{N_k+1}^{(k)}$ in terms of $\delta\mathbf{X}_0^{(k)}$ and the variable of the control parameter $\delta\sigma_0$

$$\delta\mathbf{X}_{N_k+1}^{(k)} = \mathbf{L}_x^{(k)}\delta\mathbf{X}_0^{(k)} + \mathbf{L}_u^{(k)}\delta\sigma_0, \tag{22}$$

with

$$\begin{aligned}\mathbf{L}_x^{(k)} &= \mathbf{I}_n - \mathbf{W}^{(k)}\mathbf{A}_{1:N_k}^{(k)}\left(\mathbf{D}_{1:N_k}^{(k)} - \mathbf{A}_{1:N_k}^{(k)}\right)^{-1}\mathbf{D}_0^{(k)}, \\ \mathbf{L}_u^{(k)} &= \mathbf{W}^{(k)}\left[\mathbf{A}_{1:N_k}^{(k)}\left(\mathbf{D}_{1:N_k}^{(k)} - \mathbf{A}_{1:N_k}^{(k)}\right)^{-1} + \mathbf{I}_{nN_k}\right]\mathbf{B}_{1:N_k}^{(k)},\end{aligned}$$

where $\mathbf{I}_{nN_k}$ is an identity matrix of size $nN_k \times nN_K$.

Finally, it follows from the interior point constraints that

$$\delta\mathbf{X}_{N_k+1}^{(k)} = \delta\mathbf{X}_0^{(k+1)}, \quad k = 1, 2, 3. \tag{23}$$

Combine Eq. (22) and Eq. (23) to obtain

$$\begin{aligned}\delta\mathbf{X}_{N_4+1}^{(4)} =& \mathbf{L}_x^{(4)}\mathbf{L}_x^{(3)}\mathbf{L}_x^{(2)}\mathbf{L}_x^{(1)}\delta\mathbf{X}_0^{(1)} + \\ & \{\mathbf{L}_x^{(4)}[\mathbf{L}_x^{(3)}(\mathbf{L}_x^{(2)}\mathbf{L}_u^{(1)} + \mathbf{L}_u^{(2)}) + \mathbf{L}_u^{(3)}] + \mathbf{L}_u^{(4)}\}\delta\sigma_0\end{aligned} \tag{24}$$

Since the trajectory is predicted based on the current state of motion, the variation of the initial state is always zero. Moreover, it follows from the definition of $\mathbf{B}^{(4)}$ given in Eq. (17) that $\mathbf{L}_u^{(4)} \equiv \mathbf{0}$. Hence, Eq. (24) is reduced to

$$\delta\mathbf{X}_f = \delta\mathbf{X}_{N_4+1}^{(4)} = \mathbf{L}_x^{(4)}[\mathbf{L}_x^{(3)}(\mathbf{L}_x^{(2)}\mathbf{L}_u^{(1)} + \mathbf{L}_u^{(2)}) + \mathbf{L}_u^{(3)}]\delta\sigma_0 \tag{25}$$

The linear function reveals a mapping relationship between the variation of final states and the improvement of a control parameter.

It should be noted that the coefficient matrices $\mathbf{L}_x^{(k)}$ and $\mathbf{L}_u^{(k)}$ in Eq. (25) are calculated based on the predictive trajectory information under the original control parameters. Therefore, the obtained terminal deviation is also relative to the state at the terminus of predicted trajectory. In general, especially for the problem with a fixed terminal time, $\delta\mathbf{X}_f$ can be regarded as the final state error. However, for the skip entry problem considered in this paper, $\delta\mathbf{X}_f$ needs to be further adjusted since the terminal condition of the skip phase is fixed height rather than time. Fig. (3) illustrates the process to estimate the terminal adjustment of rang-to-go s_{to-go}, which is defined as the great circle distance from the current position (θ, ϕ) to the landing site (Θ, Φ)

$$\cos(s_{to-go}) = \sin\phi\sin\Phi + \cos\Phi\cos\phi\cos(\Theta - \theta). \tag{26}$$

It is shown that a 0.172 degree increment of σ_0 at the initial point can drastically reduce s_{to-go} by 500 km. Hence, it is of great significance to accurately evaluate the terminal state error in order to obtain a precise modification of the control parameter. Let t_k denote the flight time of the predicted trajectory from the initial point at $100km$ to the second entry point at $85km$. It can be observed that the result of original transfer matrix Eq. (25) is almost same with the state

DOI: 10.13009/EUCASS2019-960

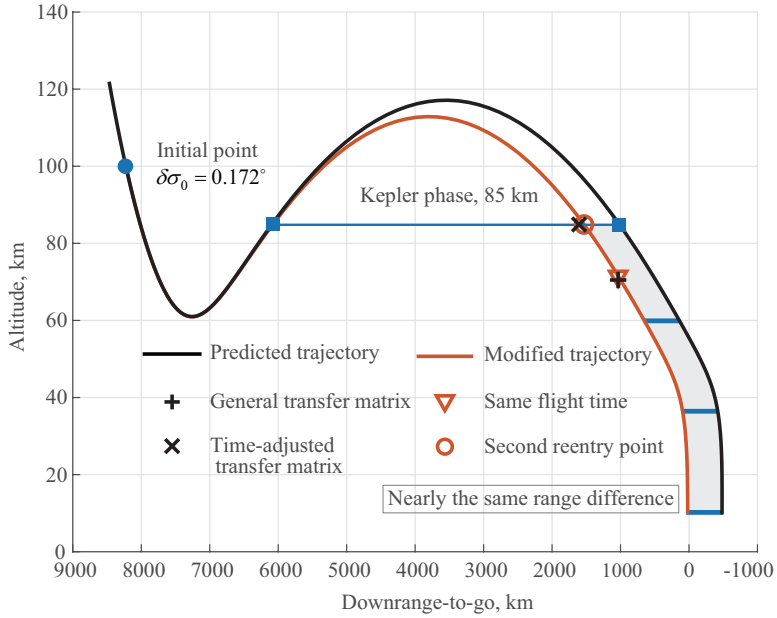

Figure 3: The estimation of adjustment at the terminal point.

of modified trajectory after the same flight time t_k. However, $\delta\mathbf{X}_f$ is not identical to the final state error of the skip phase, and the end time should be adjusted in order to be consistent with the fixed terminal height by the following expression

$$\delta t_f = \delta r_f / \dot{r}_f, \tag{27}$$

Thus the state variation at the second entry point can be formulated as

$$\delta\widehat{\mathbf{X}}_f = \delta\mathbf{X}_f + \dot{\mathbf{x}}_f \delta t_f = \mathbf{H}_f \delta\mathbf{X}_f \tag{28}$$

with

$$\mathbf{H}_f = \begin{bmatrix} 0 & 0 & 0 & 0 & 0 & 0 \\ -(\dot{\theta}/\dot{r})|_{t_f} & 1 & 0 & 0 & 0 & 0 \\ -(\dot{\phi}/\dot{r})|_{t_f} & 0 & 1 & 0 & 0 & 0 \\ -(\dot{V}/\dot{r})|_{t_f} & 0 & 0 & 1 & 0 & 0 \\ -(\dot{\gamma}/\dot{r})|_{t_f} & 0 & 0 & 0 & 1 & 0 \\ -(\dot{\psi}/\dot{r})|_{t_f} & 0 & 0 & 0 & 0 & 1 \end{bmatrix}$$

Substitute Eq. (25) into Eq. (28) to obtain

$$\delta\widehat{\mathbf{X}}_f = \mathbf{H}_f \mathbf{L}_x^{(4)} [\mathbf{L}_x^{(3)} (\mathbf{L}_x^{(2)} \mathbf{L}_u^{(1)} + \mathbf{L}_u^{(2)}) + \mathbf{L}_u^{(3)}] \delta\sigma_0 \tag{29}$$

As can be seen in Fig. (3), the result of time-adjusted transfer matrix almost coincides with the second entry point of the modified trajectory, which reflects that Eq. (29) can precisely predict the state error at the end of skip phase.

Furthermore, in order to make a more specific modification to the magnitude of initial bank angle during the skip phase, the terminal range error of the final phase is calculated by integrating differential equations Eqs. (1-6) under the condition of a constant bank angle $\sigma_f = 70\,\mathrm{deg}/s$. Since the slight adjustment $\delta\sigma_0 = 0.172\,\mathrm{deg}$ has limited influence on the initial entry velocity and the flight-path angle of the final phase, the terminal range error is nearly the same as that of the skip phase. Consequently, a correction formula can be derived for the control parameter σ_0 using Eq. (29) and the predictive terminal range error. The derivation process will be detailed later in combination with the modification of bank reversal time.

3.3 Analysis of the bank reversal time

In this subsection, the relation between terminal state errors and the modification of control parameters t_{re1} and t_{re2} is analytically derived using variation principle. As shown in Fig. (4), the state variation at the first normal bank reversal time t_{re1} can be formulated in terms of δt_{re1} as

$$\delta\mathbf{x}(t_{re1}) = \left[\mathbf{f}^{(1)}(t_{re1}) - \mathbf{f}^{(2)}(t_{re1})\right] \delta t_{re1}, \tag{30}$$

DOI: 10.13009/EUCASS2019-960

where $\mathbf{f}^{(1)}(t_{re1})$ denotes the dynamic equations before t_{re1}, while $\mathbf{f}^{(2)}(t_{re1})$ denotes the equations after t_{re1}. In this paper, the difference between $\mathbf{f}^{(1)}(t_{re1})$ and $\mathbf{f}^{(2)}(t_{re1})$ is only reflected in the sign of bank angle.

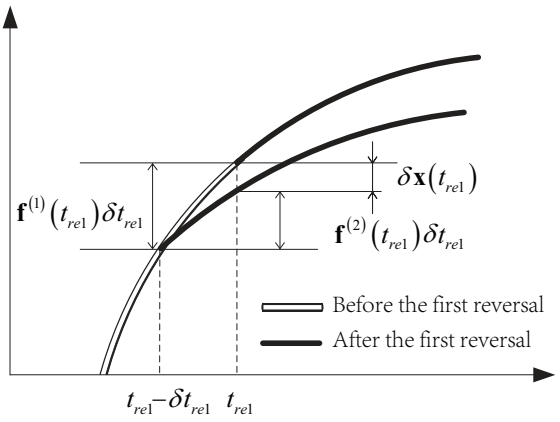

Figure 4: The variation of interior state at the first normal bank reversal time.

Since the skip entry problem is phased by the bank reversal time, $\delta\mathbf{x}(t_{re1})$ can be also regarded as the initial state variable of phase $k = 2$. Thus we have

$$\delta\mathbf{X}_0^{(2)} = \delta\mathbf{x}(t_{re1}). \tag{31}$$

It should be noted that the derivation here supposes the other control parameter is a constant, that is, $\delta\sigma_0 = 0$. Then, combine Eq. (31) with Eq. (22), Eq. (23), and Eq. (28) to obtain

$$\delta\widehat{\mathbf{X}}_f = \mathbf{H}_f\mathbf{L}_x^{(4)}\mathbf{L}_x^{(3)}\mathbf{L}_x^{(2)}\left(\mathbf{f}^{(1)}(t_{re1}) - \mathbf{f}^{(2)}(t_{re1})\right)\delta t_{re1} \tag{32}$$

Likewise, we can also analytically express the adjustment of terminal states according to the modification of the second bank reversal time as

$$\delta\widehat{\mathbf{X}}_f = \mathbf{H}_f\mathbf{L}_x^{(4)}\mathbf{L}_x^{(3)}\left(\mathbf{f}^{(2)}(t_{re2}) - \mathbf{f}^{(3)}(t_{re2})\right)\delta t_{re2} \tag{33}$$

3.4 Correction formulas

In this subsection, correction formulas are designed for the control parameters to eliminate the longitudinal and lateral errors together. Before the first bank reversal, the second bank reversal point is considered as a constant. Hence, the adjustment of terminal states can be uniformly expressed as

$$\delta\widehat{\mathbf{X}}_f = \begin{cases} \mathbf{M}^{(1)}\begin{bmatrix}\delta\sigma_0 & \delta t_{re1}\end{bmatrix}^T & t_0 \le t \le t_{re1}, \\ \mathbf{M}^{(2)}\begin{bmatrix}\delta\sigma_0 & \delta t_{re2}\end{bmatrix}^T & t_{re1} \le t \le t_{re2}, \\ \mathbf{M}^{(3)}\delta\sigma_0 & t_{re2} \le t \le t_h, \end{cases} \tag{34}$$

where

$$\begin{aligned}
\mathbf{M}^{(1)} &= \mathbf{H}_f\mathbf{L}_x^{(4)}\left[\mathbf{L}_x^{(3)}(\mathbf{L}_x^{(2)}\mathbf{L}_u^{(1)} + \mathbf{L}_u^{(2)}) + \mathbf{L}_u^{(3)} \quad \mathbf{L}_x^{(3)}\mathbf{L}_x^{(2)}\left(\mathbf{f}^{(1)}(t_{re1}) - \mathbf{f}^{(2)}(t_{re1})\right)\right], \\
\mathbf{M}^{(2)} &= \mathbf{H}_f\mathbf{L}_x^{(4)}\left[\mathbf{L}_x^{(3)}\mathbf{L}_u^{(2)} + \mathbf{L}_u^{(3)} \quad \mathbf{L}_x^{(3)}\left(\mathbf{f}^{(2)}(t_{re2}) - \mathbf{f}^{(3)}(t_{re2})\right)\right], \\
\mathbf{M}^{(3)} &= \mathbf{H}_f\mathbf{L}_x^{(4)}\mathbf{L}_u^{(3)}.
\end{aligned}$$

Since the main impacts of bank reversal time and the magnitude of initial bank angle are the lateral and longitudinal motion respectively, two terminal equality constraints are applied in the feedback control algorithm

$$\begin{aligned}
y_1 &= s_{to-go}, \\
y_2 &= \sin(\chi) = \sin(s_{to-go})\sin(\psi - \Psi),
\end{aligned}$$

with

$$\begin{aligned}
\sin\Psi &= \frac{\sin(\Theta - \theta)\cos\Phi}{\sin s_{to-go}}, \\
\cos\Psi &= \frac{\sin\Phi\cos\phi - \cos\Phi\sin\phi\cos(\Theta - \theta)}{\sin s_{to-go}},
\end{aligned}$$

DOI: 10.13009/EUCASS2019-960

Table 1: Initial skip entry conditions

h_0, km	θ_0, deg	ϕ_0, deg	V_0, km/s	γ_0, deg	ψ_0, deg
121.92	244.83	-41.13	10.98	-5.576	0.469

where y_1 denotes the terminal range adjustment of the skip phase in order to e χ is a crossrange variable, ψ is the current heading angle, and Ψ denotes the line-of-sight azimuth angle along a great circle to the landing site. As stated above, in order to satisfy the range constraint and provide a set of feasible initial conditions for the final phase, the range error of the final phase can be applied to modify the terminal range of the skip phase. Therefore, y_1 is evaluated at the terminus of simulation, while y_2 is evaluated at the terminal point of the skip phase in order to eliminate the crossrange error at the second entry point. Since the normal values of y_1 and y_2 are both zero, combine Eq. (34) to obtain

$$\begin{aligned}
\begin{bmatrix}\delta\sigma_0 & \delta t_{re1}\end{bmatrix}^T &= \left[\mathbf{Z}_1\mathbf{M}^{(1)}\right]^{-1}\begin{bmatrix}-y_1 & -y_2\end{bmatrix}^T \qquad t_0 \le t \le t_{re1},\\
\begin{bmatrix}\delta\sigma_0 & \delta t_{re2}\end{bmatrix}^T &= \left[\mathbf{Z}_1\mathbf{M}^{(2)}\right]^{-1}\begin{bmatrix}-y_1 & -y_2\end{bmatrix}^T \qquad t_{re1} \le t \le t_{re2},\\
\delta\sigma_0 &= \left[\mathbf{Z}_2\mathbf{M}^{(3)}\right]^{-1}(-y_1) \qquad\qquad\quad t_{re2} \le t \le t_h,
\end{aligned} \tag{35}$$

with

$$\begin{aligned}
\mathbf{Z}_1 &= \begin{bmatrix} 0 & \dfrac{\partial y_1}{\partial\theta} & \dfrac{\partial y_1}{\partial\phi} & 0 & 0 & 0\\ 0 & \dfrac{\partial y_2}{\partial\theta} & \dfrac{\partial y_2}{\partial\phi} & 0 & \dfrac{\partial y_2}{\partial\psi} & 0\end{bmatrix}\\
\mathbf{Z}_2 &= \begin{bmatrix} 0 & \dfrac{\partial y_1}{\partial\theta} & \dfrac{\partial y_1}{\partial\phi} & 0 & 0 & 0\end{bmatrix}
\end{aligned} \tag{36}$$

where $\mathbf{Z}_1$ and $\mathbf{Z}_2$ are coefficient matrices. The elements can be derived by taking partial derivatives to y_1 and y_2, and then given as

$$\begin{aligned}
\frac{\partial y_1}{\partial\theta} &= -\frac{1}{\sqrt{1-a^2}}\{\cos\Phi\cos\phi\sin(\Theta-\theta)\},\\
\frac{\partial y_1}{\partial\phi} &= -\frac{1}{\sqrt{1-a^2}}\{\cos\phi\sin\Phi-\cos\Phi\sin\phi\cos(\Theta-\theta)\},\\
\frac{\partial y_2}{\partial\theta} &= \cos(\Theta-\theta)\cos\psi\cos\Phi-\sin(\Theta-\theta)\sin\phi\sin\psi\cos\Phi,\\
\frac{\partial y_2}{\partial\phi} &= -\sin\phi\sin\psi\sin\Phi-\cos(\Theta-\theta)\cos\phi\sin\psi\cos\Phi,\\
\frac{\partial y_2}{\partial\psi} &= \sin(\Theta-\theta)\sin\psi\cos\Phi+\cos\phi\cos\psi\sin\Phi-\cos(\Theta-\theta)\sin\phi\cos\psi\cos\Phi,
\end{aligned}$$

with

$$a = \cos(s_{to-go}) = \sin\phi\sin\Phi+\cos\Phi\cos\phi\cos(\Theta-\theta).$$

Hence, the control parameters can be updated by the following formulations

$$\begin{aligned}
\begin{bmatrix}\sigma_0 & t_{re1}\end{bmatrix}^{k+1} &= \begin{bmatrix}\sigma_0 & t_{re1}\end{bmatrix}^{k} + \begin{bmatrix}\delta\sigma_0 & \delta t_{re1}\end{bmatrix} \qquad t_0 \le t \le t_{re1},\\
\begin{bmatrix}\sigma_0 & t_{re2}\end{bmatrix}^{k+1} &= \begin{bmatrix}\sigma_0 & t_{re2}\end{bmatrix}^{k} + \begin{bmatrix}\delta\sigma_0 & \delta t_{re2}\end{bmatrix} \qquad t_{re1} \le t \le t_{re2},\\
\sigma_0^{k+1} &= \sigma_0^{k} + \delta\sigma_0 \qquad\qquad\qquad\qquad t_{re2} \le t \le t_h
\end{aligned} \tag{37}$$

4. Evaluation of algorithm

To verify the effectiveness and robustness of the proposed method, numerical results are provided with 500 Monte Carlo simulations. The initial skip entry conditions, which correspond to a lunar-return mission with Edwards Air Force Base as the landing site, are given in Table 1. The dispersions in initial conditions and the uncertainties in aerodynamic coefficients and mass are summarized in Table 2.

In order to assess the control precision and adaptability of the proposed method, a comparison with Brunner and Lu's method is provided. Their algorithm belongs to a class of numerical guidance method. Although Fig. (5)

DOI: 10.13009/EUCASS2019-960

Table 2: Dispersion parameters

State/parameter	3σ/range	Distribution
Longitude θ_0, deg	0.2591	Gaussian
Latitude ϕ_0, deg	0.1790	Gaussian
Velocity V_0, m/ sec	13.3611	Gaussian
Flight-path angle γ_0, deg	0.1505	Gaussian
Heading angle ψ_0, deg	0.0526	Gaussian
C_L	20%	Gaussian
C_D	20%	Gaussian
Mass m, kg	±5%	Uniform

illustrates that both method can satisfy the range constraint in the longitudinal trajectory, the proposed method can predict middle states more exactly and eliminate the errors more effectively, which is clearly reflected in the control precision of the second entry point.

As shown in Fig. (6), it's apparent that the proposed method is able to control the crossrange in a succinct and accurate manner. Moreover, the lateral errors of 500 dispersed trajectories at the terminus of skip phase only have small deviations and are completely within the threshold of tolerance. By contrast, the typical method provides an irregular crossrange profile, since it is unable to predict the terminal point of skip phase precisely. Therefore, the control accuracy of the lateral error for the second entry point can not be guaranteed. It should be noted that this paper concentrates on the guidance algorithm of the skip phase, thus the final phase guidance method of Brunner and Lu is followed in this paper.

As for the bank angle profile depicted in Fig. (7), the performance of typical method is more disorder. In stark contrast, it is extremely easy to distinguish two bank reversal prescribed in the proposed method. Consequently, the guidance algorithm designed in this paper can modify the state errors more exactly with a clear concise bank angle control law.

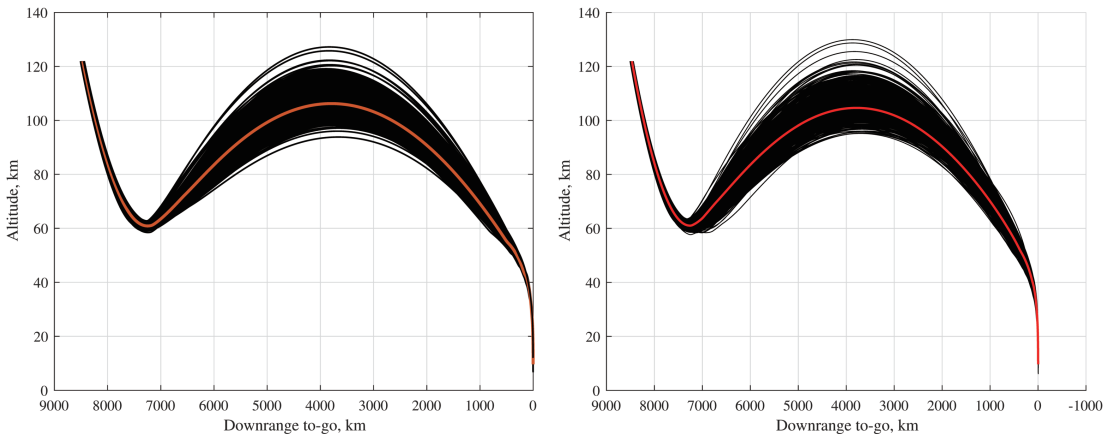

(a) The proposed method

(b) The typical method

Figure 5: Altitude versus downrange-to-go for 500 Monte Carlo runs

DOI: 10.13009/EUCASS2019-960

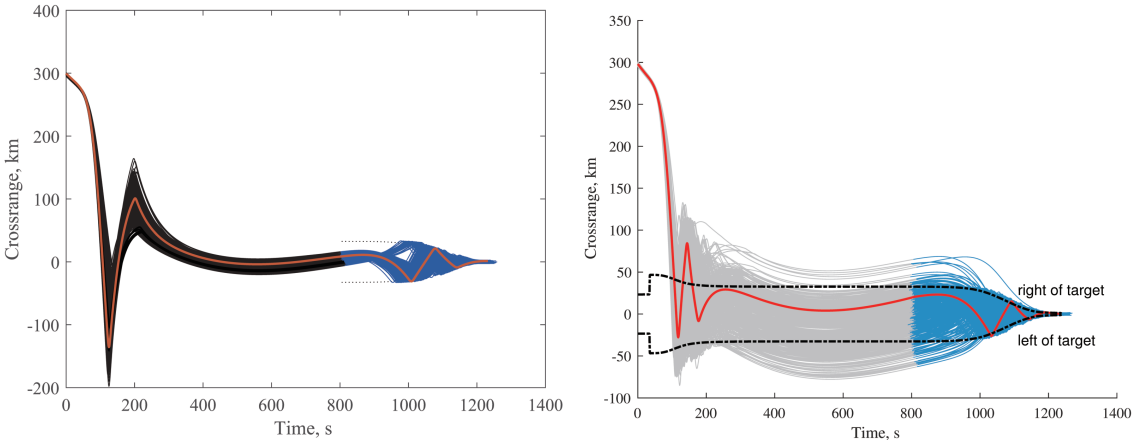

(a) The proposed method (b) The typical method

Figure 6: Crossrange profile for 500 Monte Carlo runs

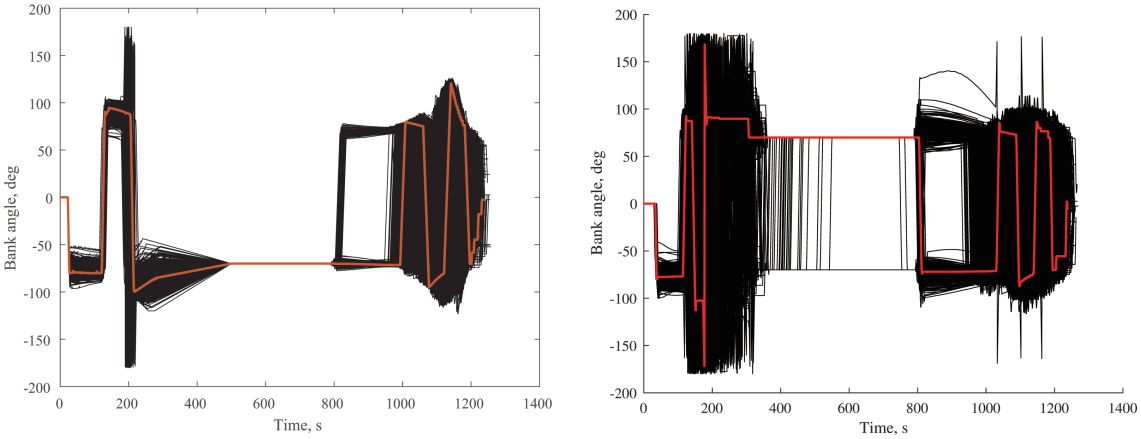

(a) The proposed method (b) The typical method

Figure 7: Bank angle profile for 500 Monte Carlo runs

DOI: 10.13009/EUCASS2019-960

Appendix

Analytical expressions of the elements in Eq. (13) are detailed as follows:

$$
\begin{aligned}
&a_{14} = \sin\gamma, && && a_{15} = V\cos\gamma;\\
&a_{21} = -\frac{V\cos\gamma\sin\psi}{r^2\cos\phi}, && && a_{23} = \frac{V\cos\gamma\sin\psi\sin\phi}{r\cos^2\phi},\\
&a_{24} = \frac{\cos\gamma\sin\psi}{r\cos\phi}, && a_{25} = -\frac{V\sin\gamma\sin\psi}{r\cos\phi}, && a_{26} = \frac{V\cos\gamma\cos\psi}{r\cos\phi};\\
&a_{31} = -\frac{V\cos\gamma\cos\psi}{r^2}, && && a_{34} = \frac{\cos\gamma\cos\psi}{r},\\
&a_{35} = -\frac{V\sin\gamma\cos\psi}{r}, && && a_{36} = \frac{V\cos\gamma\sin\psi}{r};
\end{aligned}
$$

$$
\begin{aligned}
a_{41} &= -\frac{\partial D}{\partial r} + 2\frac{\sin\gamma}{r^3} + \Omega^2\cos\phi\left(\sin\gamma\cos\phi - \cos\gamma\sin\phi\cos\psi\right),\\
a_{43} &= -\Omega^2 r\left(\sin\gamma\sin 2\phi + \cos\gamma\cos\psi\cos 2\phi\right), \quad a_{44} = -\frac{\partial D}{\partial V},\\
a_{45} &= -\left(\frac{\cos\gamma}{r^2}\right) + \Omega^2 r\cos\phi\left(\cos\gamma\cos\phi + \sin\gamma\sin\phi\cos\psi\right),\\
a_{46} &= \frac{1}{2}\Omega^2 r\cos\gamma\sin 2\phi\sin\psi;
\end{aligned}
$$

$$
\begin{aligned}
a_{51} &= \frac{1}{V}\left[\frac{\partial L}{\partial r}\cos\sigma + 2\frac{\cos\gamma}{r^3} + \Omega^2\cos\phi\left(\cos\gamma\cos\phi + \sin\gamma\cos\psi\sin\phi\right)\right],\\
a_{53} &= -2\Omega\sin\phi\sin\psi + \frac{1}{V}\Omega^2 r\left(\sin\gamma\cos\psi\cos 2\phi - \cos\gamma\sin 2\phi\right),\\
a_{54} &= \frac{\partial(L/V)}{\partial V}\cos\sigma + \left(1 + \frac{1}{rV^2}\right)\frac{\cos\gamma}{r} - \frac{1}{V^2}\Omega^2 r\cos\phi\left(\begin{matrix}\cos\gamma\cos\phi+\\ \sin\gamma\cos\psi\sin\phi\end{matrix}\right),\\
a_{55} &= \frac{\sin\gamma}{r^2V} + \frac{1}{V}\Omega^2 r\cos\phi\left(-\sin\gamma\cos\phi + \cos\gamma\cos\psi\sin\phi\right),\\
a_{56} &= 2\Omega\cos\phi\cos\psi - \frac{1}{2V}\Omega^2 r\sin\gamma\sin\psi\sin 2\phi;
\end{aligned}
$$

$$
\begin{aligned}
a_{61} &= \frac{\partial L}{\partial r}\frac{\sin\sigma}{V\cos\gamma} - \frac{V}{r^2}\cos\gamma\sin\psi\tan\phi + \frac{\Omega^2}{V\cos\gamma}\sin\psi\sin\phi\cos\phi,\\
a_{63} &= \frac{V}{r\cos^2\phi}\cos\gamma\sin\psi + 2\Omega\left(\tan\gamma\cos\psi\sin\phi + \cos\phi\right) + \frac{\Omega^2 r}{V\cos\gamma}\sin\psi\cos 2\phi,\\
a_{64} &= \frac{\partial(L/V)}{\partial V}\frac{\sin\sigma}{\cos\gamma} + \frac{\cos\gamma\sin\psi\tan\phi}{r} - \frac{\Omega^2 r}{V^2\cos\gamma}\sin\psi\sin\phi\cos\phi,\\
a_{65} &= \frac{L\sin\sigma}{V\cos^2\gamma}\sin\gamma - \frac{V}{r}\sin\gamma\sin\psi\tan\phi - \frac{2\Omega\cos\psi\cos\phi}{\cos^2\gamma} + \frac{\Omega^2 r}{V\cos^2\gamma}\sin\gamma\sin\psi\sin\phi\cos\phi,\\
a_{66} &= \frac{V}{r}\cos\gamma\cos\psi\tan\phi + 2\Omega\tan\gamma\sin\Psi\cos\phi + \frac{\Omega^2 r}{V\cos\gamma}\cos\psi\sin\phi\cos\phi;
\end{aligned}
$$

and

$$
b_{51} = -\frac{L}{V}\sin\sigma, \qquad b_{61} = \frac{L\cos\sigma}{V\cos\gamma},
$$

where the partial derivatives of the aerodynamic forces D and L with respect to the radial distance r and the relative velocity V are given as

$$
\begin{aligned}
\frac{\partial D}{\partial r} &= \frac{D}{\rho}\frac{\partial\rho}{\partial r}, & \frac{\partial D}{\partial V} &= \frac{2D}{V},\\
\frac{\partial L}{\partial r} &= \frac{L}{\rho}\frac{\partial\rho}{\partial r}, & \frac{\partial\left(L/V\right)}{\partial V} &= \frac{L}{V^2}.
\end{aligned}
$$

DOI: 10.13009/EUCASS2019-960

It should be noted that the partial derivatives of C_L and C_D are not considered in the derivation, since only hypersonic velocities are involved in the skip phase and the aerodynamic coefficients are nearly constant.

References

[1] Christopher W. Brunner and Ping Lu. Skip Entry Trajectory Planning and Guidance. *Journal of Guidance, Control, and Dynamics*, 31(5):1210–1219, September 2008.

[2] Claude A. Graves and Jon C. Harpold. Apollo experience report: Mission planning for Apollo entry. Technical Report NASA-TN-D-6725, March 1972.

[3] Craig A. Kluever. Entry Guidance Using Analytical Atmospheric Skip Trajectories. *Journal of Guidance, Control, and Dynamics*, 31(5):1531–1535, September 2008.

[4] Ping Lu. Predictor-Corrector Entry Guidance for Low-Lifting Vehicles. *Journal of Guidance, Control, and Dynamics*, 31(4):1067–1075, July 2008.

[5] Ping Lu, Christopher W. Brunner, Susan J. Stachowiak, Gavin F. Mendeck, Michael A. Tigges, and Christopher J. Cerimele. Verification of a Fully Numerical Entry Guidance Algorithm. *Journal of Guidance, Control, and Dynamics*, 40(2):230–247, February 2017.

[6] Zong-Fu Luo, Hong-Bo Zhang, and Guo-Jian Tang. Skip entry guidance using numerical predictor–corrector and patched corridor. *Acta Astronautica*, 117:8–18, December 2015.

[7] Richard Orloff and Stephen Garber. *Apollo by the Numbers: A Statistical Reference*. January 2000.

[8] Z. R. Putnam, S. H. Bairstow, R. D. Braun, and G. H. Barton. Improving Lunar Return Entry Range Capability Using Enhanced Skip Trajectory Guidance. *Journal of Spacecraft and Rockets*, 45(2):309–315, March 2008.

[9] Z. R. Putnam, R. D. Braun, R. R. Rohrschneider, and J. A. Dec. Entry System Options for Human Return from the Moon and Mars. *Journal of Spacecraft and Rockets*, 44(1):194–202, January 2007.

[10] Zachary R. Putnam, Matthew D. Neave, and Gregg H. Barton. PredGuid entry guidance for Orion return from low Earth orbit. In *2010 IEEE Aerospace Conference*, pages 1–13, Big Sky, MT, USA, March 2010. IEEE.

[11] Jeremy Rea and Zachary Putnam. A Comparison of Two Orion Skip Entry Guidance Algorithms. In *AIAA Guidance, Navigation and Control Conference and Exhibit*, Hilton Head, South Carolina, August 2007. American Institute of Aeronautics and Astronautics.

[12] Tao Wang, Hongbo Zhang, Liang Zeng, and Guojian Tang. A robust predictor–corrector entry guidance. *Aerospace Science and Technology*, 66:103–111, July 2017.

[13] Liang Yang, Xiaoming Liu, Wanchun Chen, and Hao Zhou. Autonomous entry guidance using Linear Pseudospectral Model Predictive Control. *Aerospace Science and Technology*, 80:38–55, September 2018.

[14] Bo Zhang, Shuo Tang, and Binfeng Pan. Automatic load relief numerical predictor-corrector guidance for low L/D vehicles return from low Earth orbit. *Proceedings of the Institution of Mechanical Engineers, Part G: Journal of Aerospace Engineering*, 229(11):2106–2118, September 2015.